

Towards Synthesized and Editable Motion In-Betweening Through Part-Wise Phase Representation

Minyue Dai^{1,2} Ke Fan³ Bin Ji³ Haoran Xu⁴ Haoyu Zhao⁵

Junting Dong² Jingbo Wang² Bo Dai⁶

¹Fudan University ²Shanghai Artificial Intelligence Laboratory ³Shanghai Jiaotong University

⁴Zhejiang University ⁵Wuhan University ⁶University of Hong Kong

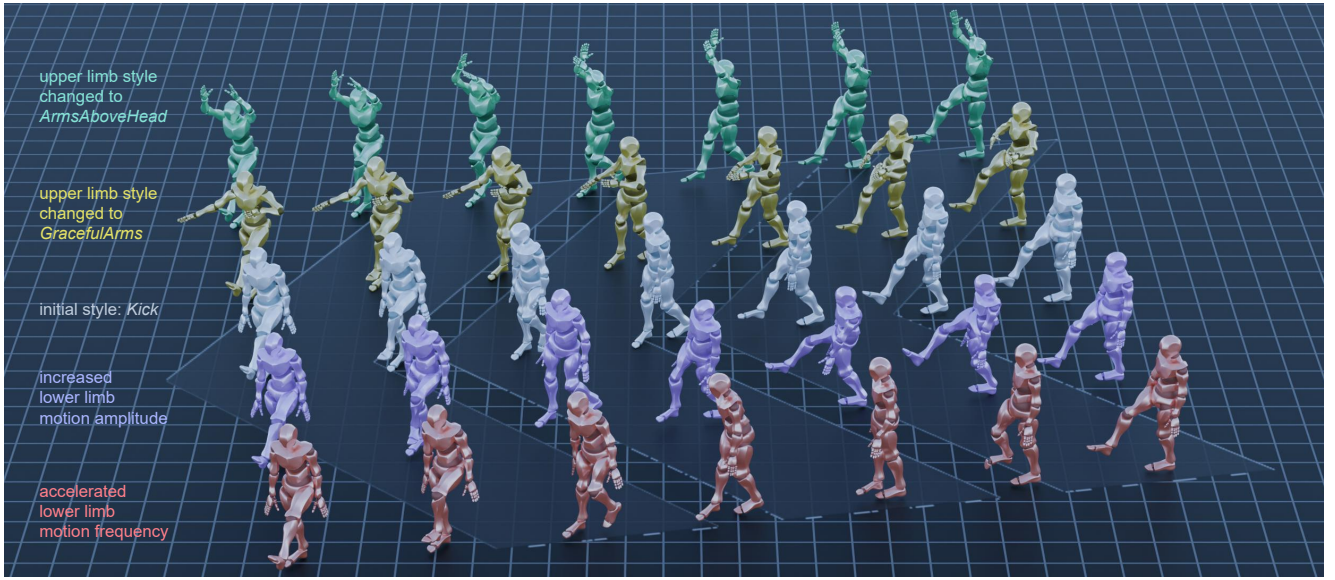


Figure 1. We demonstrate the effectiveness of our framework in generating stylized online motion in-between. It excels at producing realistic animations that accurately reflect the target style during variations in body part movements, while also allowing adjustments to the individual body parts or overall movements. These capabilities make our framework a robust and versatile solution for stylized in-between generation through part-aware phase representation.

Abstract

Stylized motion in-betweening is crucial for computer animation and gaming. However, existing methods typically encode motion styles by modeling whole-body motions, often overlooking the representation of individual body parts. This limitation reduces the flexibility of in-filled motion, particularly in adjusting the motion styles of specific limbs independently. To overcome this challenge, we propose a novel framework that models motion styles at the body-part level, enhancing both the diversity and controllability of in-filled motions. Our approach enables more nuanced and expressive animations by allowing precise modifications to individual limb motions while maintaining overall motion coherence. Leveraging phase-related insights, our frame-

work employs periodic autoencoders to automatically extract the phase of each body part, capturing distinctive local style features. Additionally, we effectively decouple the motion source from synthesis control by integrating motion manifold learning and conditional generation techniques from both image and motion domains. This allows the motion source to generate high-quality motions across various styles, with extracted motion and style features readily available for controlled synthesis in subsequent tasks. Comprehensive evaluations demonstrate that our method achieves superior speed, robust generalization, and effective generation of extended motion sequences.

1. Introduction

Motion in-betweening is a fundamental technique for generating complete motion sequences from sparse keyframe poses. It serves as a cornerstone for numerous applications in computer vision and computer graphics, including character animation [40, 41], action recognition, and motion capture. The diversity and controllability of in-between motion are of paramount importance, as they directly influence the realism, expressiveness, and adaptability of synthesized motion. In this work, we introduce a novel approach to fine-grained style control in motion in-betweening, explicitly focusing on the independent manipulation of motion styles across different body parts.

Early methods formulated in-between motions as a motion planning problem [34, 35, 38]. In the context of deep learning, in-between motion is framed as a task within motion manifold learning [5, 10, 32, 36] or as a control problem using temporal control signals [19]. However, without precise style control, character motion transitions generated by these methods often default to the most probable motion, misaligning with the intended style. Although some recent approaches encode style information from entire motion sequences [33], they inadequately capture body part style features, particularly during stylistic changes. This limitation results in generating the most probable motion rather than the desired stylistic expression when adjusting motion of body parts. Furthermore, these methods do not allow for adjusting of body part motions.

To address this issue, we propose a novel framework for stylized online motion in-betweening that significantly enhances the diversity and controllability of in-between motion styles. Our method draws on phase-related techniques, utilizing periodic autoencoders [31] to automatically extract parameters such as frequency amplitudes and motion velocities within the motion latent space, ensuring high-quality in-between motion. However, existing approaches typically extract phase information from the entire body, limiting precise style control over specific body parts during in-between motion, such as maintaining lower body motion while altering upper body dynamics.

Therefore, our framework first extracts local phases of body parts using the character’s kinematic chain, enabling individual modeling of the motion latent space for each limb. Leveraging this pre-captured latent space, we propose our framework to infill motion at the subsequent time step with an additional motion sampler. To better align the motion style with part-level motions, we encode the motion style through body part phases, effectively capturing specific stylistic attributes without relying on the whole body representation [21, 33]. This approach accurately reflects the target style during changes in body part motions, such as raising legs while keeping hands behind the back, thereby unlocking the potential for fine-grained

style control in the in-between motion. Consequently, our method demonstrates superior generalization capabilities. The fine-grained phase representation facilitates nuanced adjustments to the amplitude of individual body parts or overall motion. We can modify motion characteristics by scaling the amplitude and frequency of the body part phases while preserving overall body coordination. Extensive experiments on the 100STYLE dataset [21] demonstrate that our method can *controls motion of body part motion*, ensuring consistent style adherence in long sequences and style transitions. In summary, our work makes the following contributions:

- We introduce body part-based phase features, enhancing motion generation quality for long sequences.
- We propose a style encoder based on body part phases that captures the stylistic information of body parts.
- Our model allows for the adjustment of both the magnitude and frequency of body part motions.

2. Related Works

In-between motion synthesis. In-between motion synthesis can be formulated as a motion planning problem [2, 3, 16, 26, 34], which involves solving complex optimization problems under various constraints. Data-driven methods improve efficiency and enhance motion naturalness by searching structured data such as motion graphs [15, 22, 27]. As the field of neural networks continues to advance, some methodologies have emerged that focus on learning the motion manifold [5, 8, 9, 12, 17, 23–25, 36] to synthesize motions using various control signals [6]. Harvey et al. [7] proposed a neural network capable of generating plausible intermediate motions between given keyframe poses. Their primary contribution lies in strengthening the relationship between motion and time by embedding temporal information. Building upon this, Tang et al. [32] introduced Convolutional Variational Autoencoder (CVAE) to further explore the impact of temporal information. SKEL-Betweeners [1] generates extended motion sequences from two poses using neural motion curves (intuitive joint-level controls for positioning and orientation). Our phase-based control approach complements trajectory-level methods: whereas prior work [1] ensures precision through spatiotemporal curves, our method maintains natural coordination by leveraging biomechanically constrained phase parameters. This enables style-consistent editing (e.g., adjusting arm swing magnitude throughout dance sequences) without requiring manual coordination efforts.

Phase. Previous motion interpolation techniques struggled to adapt to longer durations between keyframes due to the generalization effects of temporal information. The first successful exploration of this issue was presented in the Phase-Functioned Neural Networks (PFNN) [11]. It

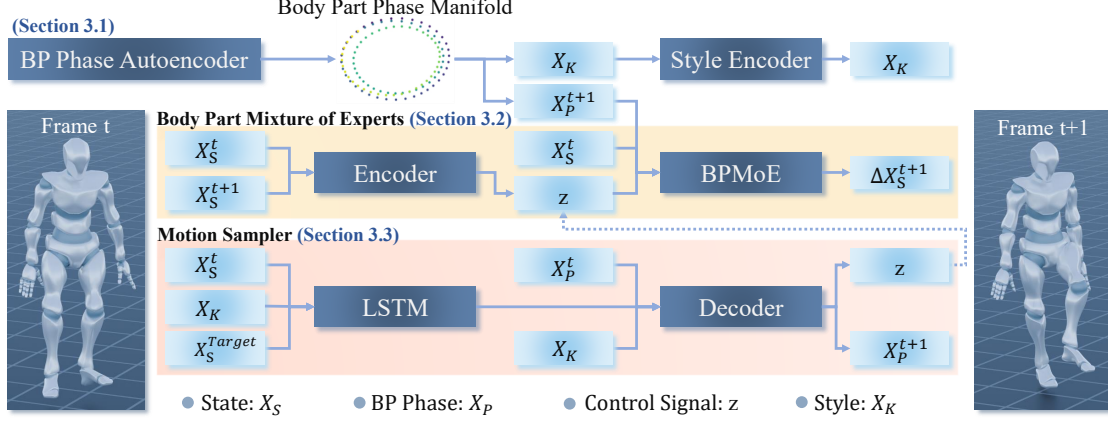


Figure 2. **System Overview.** We first train the BP Phase Autoencoder (Body Part Phase Autoencoder) similar to [31]. Next, we train the BPMoE (Body Part Mixture of Experts). The encoder takes the current state and the next state to generate the control signal. BPMoE takes the control signal, the current state, and the next BP Phase to predict the next state. Finally, when training the Motion Sampler, we remove the encoder, fix BPMoE and connect the Motion Sampler to BPMoE. The style encoder encodes the BP Phase into style information. The LSTM network takes the current, target state, and style information as input, and the output is decoded into control signals and the next BP Phase, along with the current BP Phase and style information.

utilizes phase-controlled neural motion controllers to interpolate human motion behaviors. Based on this approach, Starke et al. [29] proposed representing different motion skills through multiple phase variables, enabling the model to effectively learn a vast array of motions. Subsequently, Starke et al. [30] delved into phase representation, introducing a contact-based method for phase extraction at the local joint level. However, this approach is limited to movements involving physical contacts. Many motions, especially those of the hands, lack such contacts, making phase definition a challenging problem. Another challenge with phases based on contacts is that they require careful tuning of thresholds for computing the phase labels. Mason et al. [21] use a PCA heuristic to compute the local phase of cyclic arm movements during locomotion, although a different heuristic would be needed for arbitrary movements. Recently, research has shifted towards learning-based phase extraction to achieve spatiotemporal alignment for arbitrary character motions [31]. This method learns multi-dimensional phase variables from arbitrary unstructured motion capture data. However, it extracts phase information from the entire body, which limits precise style control over individual body parts. We further investigate the impact of learning-based phase extraction at the body-part level on motion quality, as well as the effects of body-part phase alterations on motion generation. Additionally, we analyze the relationship between phase and motion style in greater depth.

3. Methodology

To overcome the limitations of existing methods that encode motion styles holistically and lack precise part-level control [7, 28, 32, 33], our framework introduces a body-part decomposition strategy inspired by phase dynamics in human motion [31]. Our framework comprises three distinct components: the **BP Phase Autoencoder** (Body Part Phase Autoencoder), the **BPMoE** (Body Part Mixture of Experts) and the **Motion Sampler**. First, we present the BP Phase Autoencoder, which extracts body-part phases from motion data (Section 3.1). Next, the BPMoE generates the next frame’s state based on the current frame’s state and the control signal (Section 3.2). Finally, the Motion Sampler produces a control signal that aligns with the target frame, the desired transition duration, and style information (Section 3.3).

3.1. Body Part Phase Autoencoder

Motion in-betweening fundamentally relies on temporally coherent transitions [7, 28, 32, 33, 42]. The phase variable intrinsically encodes motion dynamics by modeling cyclic patterns [11, 30, 31]. However, conventional implementations rely on whole-body monolithic representations for phase extraction [33], leading to phase entanglement, where distinct limb kinematics are coupled in latent space. This architectural limitation fundamentally restricts fine-grained control over individual body parts during motion synthesis. We propose part-specific temporal autoencoders that map body motions to localized phase manifolds. The BP Phase Autoencoder takes a sequence of motion data within a specified time window $\mathbf{M} = \{X_S^0, \dots, X_S^T\}$ as

input and outputs the phases $\mathbf{X}_{\mathcal{P}}^t = \{\Theta_1^t, \Theta_2^t, \dots, \Theta_n^t\}$. $\mathbf{X}_S^t = \{p^i, v^i, r^i\}$ includes bone positions $p^i \in \mathbb{R}^{3B}$, bone rotations $r^i \in \mathbb{R}^{6B}$, and bone velocities $v^i \in \mathbb{R}^{3B}$, where B represents the number of joints. $\Theta_i \in \mathbb{R}^{2m}$ represents the phase information for the i th body part. n and m represent the number of body parts and the number of channels for body part phases, respectively.

We structure the latent space with explicit periodic constraints. Each body part's phase vector Θ_i is parameterized by:

$$\Theta_i^{2j-1} = A_i^j \cdot \sin(2\pi \cdot S_i^j), \Theta_i^{2j} = A_i^j \cdot \cos(2\pi \cdot S_i^j), \quad (1)$$

where $A_i^j \in \mathbb{R}^+$ represents the magnitude and could control the motion amplitude, and $S_i^j \in [0, 1)$ as the angular progression, could regulate timing for the j th phase channel of the i th body part.

3.2. Body Part Mixture of Experts

Traditional motion generation systems typically rely on a single network to handle all body parts simultaneously[7], potentially leading to conflicting control signals. Our BPMoE solves this problem by employing specialized sub-networks for distinct biomechanical patterns, dynamically fused through phase-synchronized gating. It preserves localized motion fidelity while maintaining global coordination. The BPMoE predicts the incremental change between frames based on the posture, control signal, and body part phases at the current frame t , which is formulated as:

$$\mathbf{X}_S^{t+1} = \mathbf{X}_S^t + \text{BPMoE}(z^{t+1}, \mathbf{X}_S^t, \mathbf{X}_{\mathcal{P}}^t), \quad (2)$$

where the control signal $z \in \mathbb{R}^{32}$ governs the system's dynamics, and $\mathbf{X}_K \in \mathbb{R}^{111 \times 512}$ captures style attributes.

During training, the encoder transforms two successive frames $\mathbf{X}_S^t, \mathbf{X}_S^{t+1}$ into z^t , which is restricted within the range $z \sim \mathcal{N}(0, 1)$ to capture the stochasticity of transition. The gating network establishes a weighting mechanism for experts based on the provided input. It considers the phases extracted from the body part phase manifold and the control signal to calculate blending coefficients for the experts. The final output is a weighted combination of outputs generated by all participating experts.

3.3. Motion Sampler

The Motion Sampler serves as a parametric controller that resolves spatio-temporal constraints. It receives inputs including the current frame \mathbf{X}_S^t , the target frame $\mathbf{X}_S^{T_{\text{target}}}$, the phase of the current body part $\mathbf{X}_{\mathcal{P}}^t$ and the target style \mathbf{X}_K . Subsequently, it generates the control signal z^t , which can be further used in the BPMoE (Section 3.2) to sample the following frame.

Given that the phase effectively captures stylistic information, we utilize the body part phases as input for the style

encoder. We first extract a style code from the body part phases using the style encoder based on convolutional neural networks: $\mathbf{X}_K = E_{\text{style}}(\Theta_1, \Theta_2, \dots, \Theta_n)$. By separating and encoding the comprehensive body motion sequence into individual body part motion phases, we can discern styles for each body part. Then, we use a long-short-term memory (LSTM) network to derive the next state, which is then integrated into the decoder along with the phase $\mathbf{X}_{\mathcal{P}}^t$ and the style code \mathbf{X}_K . This process yields the control signal z^t , which is subsequently utilized within the BPMoE framework to sample the next frame.

For every body part, we anticipate an intermediate subsequent phase $\hat{\Theta}^{t+1}$, along with estimating the amplitude \hat{A}^{t+1} and frequency \hat{F}^{t+1} . An additional intermediate phase vector is calculated as follows: $\tilde{\Theta}^{t+1} = \hat{A}^{t+1} \cdot (R(2\pi \Delta t \hat{F}^{t+1}) \cdot \Theta^t)$, where Δt denotes the time step, and R represents a 2D rotation matrix. We apply spherical linear interpolation with a weight of 0.5 to interpolate the angles of $\tilde{\Theta}^{t+1}$ and $\hat{\Theta}^{t+1}$, followed by linear interpolation with the same weight for the final prediction Θ^{t+1} .

3.4. Training.

Our framework employs a two-stage training strategy to progressively optimize motion quality. The first stage trains the BPMoE, followed by the training of the motion sampler in the second stage. When training the Motion Sampler, we remove the encoder, fix BPMoE and connect the Motion Sampler to BPMoE.

The first stage trains the BPMoE using three fundamental components. **Reconstruction Loss** (L_{rec}): The L2 distance $\|\mathbf{X}_S - \mathbf{X}_S'\|_2^2$ between predicted (\mathbf{X}_S') and ground truth (\mathbf{X}_S) joint parameters enforces precise pose reconstruction, preserving local limb geometries and global body coordination. **Latent Regularization** (L_{kl}): The KL-divergence term $-\frac{1}{2}(1 + \sigma^2 - \mu^2 - e^\sigma)$ regularizes the control signal distribution $z \sim \mathcal{N}(0, 1)$, preventing overfitting while maintaining a smooth latent space for diverse motion sampling. The hyperparameter $\beta = 0.001$ balances reconstruction accuracy and generative diversity [32]. **Foot Plant Constraint** (L_{foot}): To eliminate foot sliding, we introduce $\|f_v' \odot \delta(v_f)\|_2^2$ where $\delta(v_f)$ implements velocity-dependent contact weighting. The composite BPMoE objective integrates these components:

$$\mathcal{L}_{\text{BPMoE}} = L_{\text{rec}} + \beta L_{\text{kl}} + L_{\text{foot}}. \quad (3)$$

For the motion sampler, we extend the loss formulation with temporal and phase-aware terms: **Temporal Consistency** (L_{rec}): L1 distance $\|\mathbf{X}_S - \mathbf{X}_S'\|_1$ ensures robust frame-to-frame coherence under motion variations. **Keyframe Alignment** (L_{last}): Strict terminal constraint $\|\mathbf{X}_S^T - (\mathbf{X}_S')^T\|_1$ enforces precise matching of the final generated frame to the target pose. **Phase Dynamics** (L_{phase}):

Maintains limb-specific motion characteristics through:

$$\|A - \hat{A}\|_2^2 + \|F - \hat{F}\|_2^2 + \frac{1}{2}(\|p - \hat{p}\|_2^2 + \|p - \tilde{p}\|_2^2) \quad (4)$$

, where phase velocity F^t preserves cyclic continuity via: $F^t = (S^t - S^{t-1}) - \lfloor S^t - S^{t-1} + 0.5 \rfloor$. The sampler’s total loss combines these objectives:

$$\mathcal{L}_{\text{Sampler}} = L_{\text{rec}} + L_{\text{last}} + \lambda_{\text{foot}} L_{\text{foot}} + \lambda_{\text{phase}} L_{\text{phase}}. \quad (5)$$

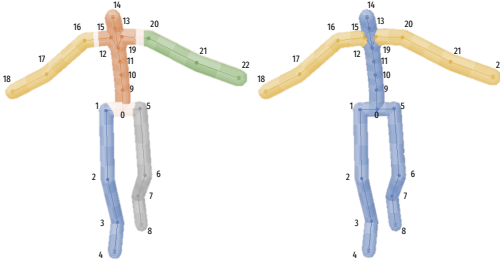


Figure 3. The five body parts of the first method consist of the left upper limb (joints 15 to 18), right upper limb (joints 19 to 22), left lower limb (joints 1 to 4), right lower limb (joints 5 to 8), and the torso (joints 9 to 12). The second method requires the selection of two body parts: the upper limbs (joints 15 to 22) and the other segments (joints 0 to 14).

4. Experiments

In this section, we first describe our experimental setup and evaluation metrics. Next, we analyze the effectiveness of the proposed framework. Finally, we showcase our method’s capability for parametric control of limb motion characteristics through amplitude-frequency modulation in synthesized animations.

4.1. Experimental Settings

Body part grouping. Human motion possesses inherent structural characteristics due to inter-joint coordination. We implement two physiologically-grounded body part divisions (Fig.3): (1) The bipartite decomposition follows biomechanical principles from [14, 20], separating upper and lower extremities to preserve limb-specific dynamics; (2) The five-segment scheme builds upon kinematic chain analyses in [1, 4, 18, 37], isolating torso, bilateral arms and legs to capture finer motion semantics. This explicit part-wise decomposition facilitates the decoupling of movement patterns while preserving physiological coordination, providing a significant advantage over automated skeleton-aware convolutions [1] for phase-based motion editing.

Dataset. Following [33], we utilize the 100STYLE motion dataset [21]. We remove all wrist and thumb joints

to retarget the motion to a skeleton with 23 joints. Additionally, we downsample the motion sequences to 30 fps and augment them using mirroring and random time cropping [13]. We clip the motion manifold into segments of 120 frames, with each segment overlapping by 20 frames. The motion orientation is adjusted so that the first frame faces the X-axis [10]. We employ global joint directions rotating along a forward and upward vector $r \in \mathbb{R}^6$ [39]. The motion $\mathbf{M} \in \mathbb{R}^{23 \times 12 \times 120}$ encompasses global joint positions (\mathbb{R}^3), velocities (\mathbb{R}^3), and rotations (\mathbb{R}^6).

Metrics. We evaluate the movements in terms of reconstruction accuracy and foot skating artifacts. The reconstruction accuracy is calculated using the averaged L2 distance of global joint positions and the Normalized Power Spectrum Similarity (NPSS) in the joint angle space [7]. The foot skating artifacts [39] are quantified based on the averaged foot velocity v_f when the foot height h is below a threshold $H = 2.5$: $L_f = v_f \cdot \text{clamp}(2 - 2^{h/H}, 0, 2)$.

Implementation Details. Our **network architecture** is configured as follows: The Body Part Mixture of Experts (BPMoE) employs 8 parallel expert networks. All encoder modules (excluding the style encoder) follow an identical structure: a feed-forward network comprising one hidden layer of 512 neurons and an output layer of 256 neurons, with PLU activation applied after each linear transformation. The temporal modeling component utilizes an LSTM with 1024 hidden units for motion sequence processing. The phase decoder architecture consists of two successive feed-forward layers – the first with 512 units and the second with 256 units – both employing Exponential Linear Unit (ELU) activation functions.

To accelerate training convergence, we randomly select a 25-frame window from the 120-frame clips for each step instead of using the full sequence. We employ AMSGrad with parameters ($\beta_1 = 0.5, \beta_2 = 0.9$) and a learning rate of $1e - 3$. For training the sampler, we shuffle all style sequences randomly. To ensure model robustness across varying time lengths, we randomly sample a sequence starting at a length of 20 frames and linearly increase it to 40 frames at each epoch, similar to [7]. We use the same AMSGrad setup as before, with a weight decay of $1e - 4$ for training the style encoder to prevent overfitting, while the weight decay for other modules is set to 0. After training the BPMoE, we remove its encoder, fix its decoder, and connect the motion sampler to the fixed decoder to train the sampler. This training process typically takes around a day. We conduct our experiments using an NVIDIA 4090 24G GPU. Our method takes, on average, 1.87 ms to synthesize one frame, which is sufficient for real-time applications.

Metrics	NPSS(\downarrow)			L2 norm of global position(\downarrow)			skating(\downarrow)		
Frames	120	140	160	120	140	160	120	140	160
CVAE	7.179	10.788	14.645	27.936	34.322	39.731	0.127	0.111	0.097
RSMT	7.378	10.311	13.981	25.848	32.082	36.664	0.137	0.129	0.116
PhaseMIB	7.133	10.512	12.171	25.768	31.586	35.798	0.142	0.132	0.126
OURS(2)	6.780	9.443	12.178	25.300	30.052	35.185	0.116	0.100	0.093
OURS(5)	7.800	10.909	14.626	25.816	31.118	35.746	0.094	0.083	0.074

Table 1. Comparison on reconstruction and foot skating metrics of different methods.

NPSS (\downarrow)	upper limbs			left upper limb			right upper limb		
Frames	120	140	160	120	140	160	120	140	160
CVAE	7.279	10.968	14.821	7.289	10.852	14.763	7.253	10.901	14.817
RSMT(original)	7.266	10.525	14.113	7.312	10.567	14.038	7.384	10.453	14.178
RSMT(modified)	7.297	10.426	13.909	7.221	10.466	13.918	7.372	10.521	14.197
PhaseMIB	7.158	10.524	12.985	7.667	10.686	12.769	7.731	10.705	12.810
OURS(2)	6.938	9.633	12.364	6.928	9.603	12.333	6.885	9.634	12.307
OURS(5)	7.779	10.943	14.710	7.795	10.950	14.455	7.913	11.075	14.672
L2 norm (\downarrow)	upper limbs			left upper limb			right upper limb		
	120	140	160	120	140	160	120	140	160
CVAE	28.343	34.586	40.027	28.220	34.440	40.036	28.256	34.621	39.970
RSMT(original)	26.314	32.333	36.925	26.087	32.196	36.899	26.233	32.297	37.042
RSMT(modified)	26.255	32.303	36.998	26.074	32.164	36.790	26.185	32.219	37.033
PhaseMIB	27.124	31.714	35.946	26.537	33.322	36.754	27.934	34.386	36.967
OURS(2)	26.027	30.781	35.701	25.798	30.518	35.387	25.675	30.451	35.454
OURS(5)	26.113	31.543	36.242	25.995	31.424	36.029	26.162	31.342	35.969
Skating (\downarrow)	upper limbs			left upper limb			right upper limb		
	120	140	160	120	140	160	120	140	160
GT	0.044	0.044	0.044	0.044	0.044	0.044	0.044	0.044	0.044
CVAE	0.132	0.114	0.100	0.130	0.112	0.099	0.130	0.113	0.100
RSMT(original)	0.141	0.134	0.120	0.141	0.134	0.122	0.138	0.130	0.117
RSMT(modified)	0.141	0.131	0.119	0.142	0.130	0.120	0.138	0.129	0.118
PhaseMIB	0.146	0.139	0.126	0.152	0.137	0.130	0.154	0.143	0.137
OURS(2)	0.115	0.105	0.094	0.115	0.102	0.091	0.116	0.105	0.093
OURS(5)	0.099	0.085	0.078	0.095	0.083	0.076	0.099	0.086	0.077

Table 2. Comparison of reconstruction and foot skating metrics for different methods with changes in body part styles

4.2. Comparison with State-of-the-Arts

Comparison under Seen Styles. We evaluate our framework against CVAE [32], RSMT [33] and PhaseMIB [28] on the 100STYLE dataset, with results in Table 1. For short sequences, RSMT [33] and CVAE [32] exhibit better controllability due to their interpolation-focused design that minimizes temporal feature complexity. However, this simplification becomes detrimental for longer sequences, where CVAE [32]’s insufficient temporal modeling and RSMT [33]’s ineffective temporal encoding lead to performance degradation. While PhaseMIB [28] improves long-sequence generation through bidirectional control, its

whole-body phase representation intrinsically couples limb dynamics, causing style entanglement that limits part-wise motion control, which is a fundamental limitation shared with prior approaches.

Our approach decouples full-body movements and captures temporal information that better aligns with human structural characteristics. Therefore, when confronted with tasks requiring the generation of long sequences, we excel in controllability and motion quality. Specifically, dividing the body into two parts accounts for the collaborative effects of the upper and lower body separately, leading to a better representation of overall frequency domain information and resulting in superior performance on the NPSS metric. Di-

Metrics	NPSS(\downarrow)			L2 norm of global position(\downarrow)			skating(\downarrow)		
Frames	120	140	160	120	140	160	120	140	160
Motion-based	7.573	10.927	14.616	27.551	32.609	37.184	0.148	0.126	0.109
OURS(2)	6.780	9.443	12.178	25.300	30.052	35.185	0.116	0.100	0.093
OURS(5)	7.800	10.909	14.626	25.816	31.118	35.746	0.094	0.083	0.074

Table 3. Comparisons of reconstruction and foot skating between motion-based and body-part-phase-based representation.

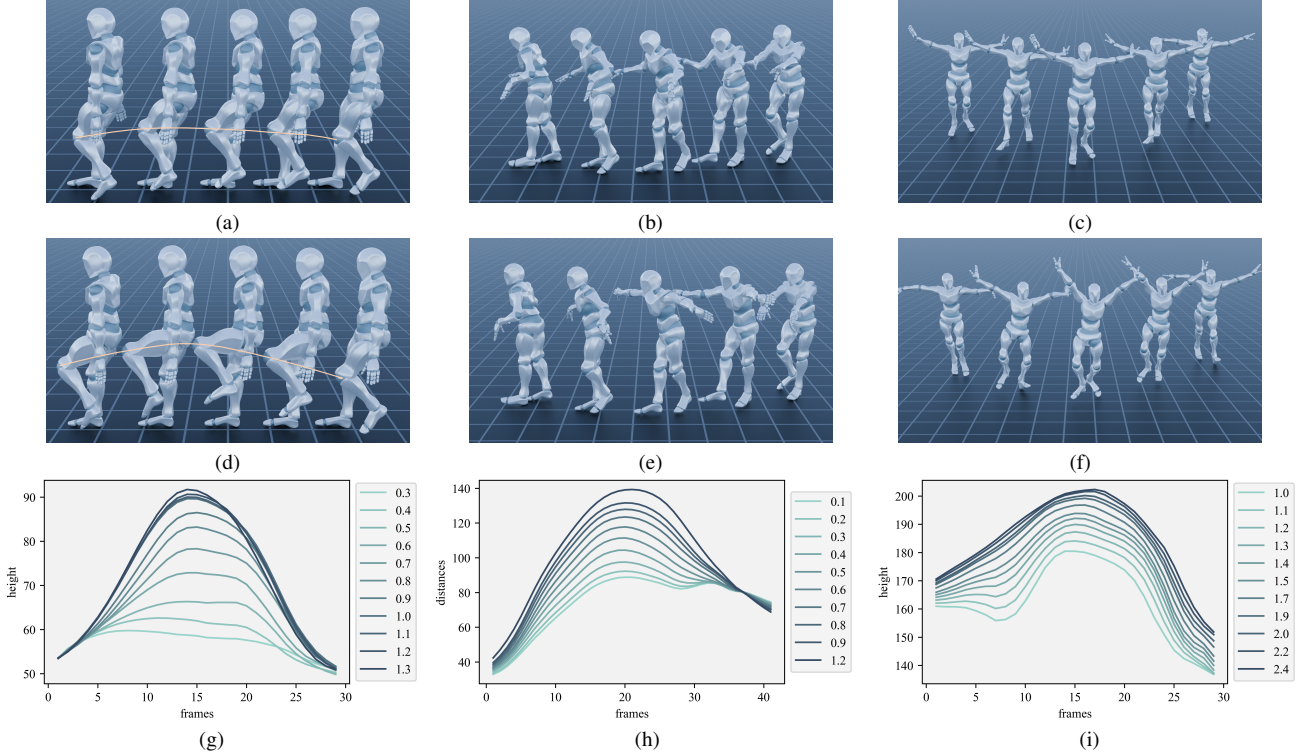


Figure 4. Results of adjusting the amplitude of body part phases

viding the body into five parts further captures the intrinsic periodicity of the limbs, enhancing the frequency domain representation for individual limbs and thereby outperforming the skating metric. As both models excel in representing temporal information, they surpass baseline in terms of the averaged L2 distance of global joint positions.

Comparison under Unseen Styles. We evaluate our method’s generalization to unseen styles caused by body part modifications. Three test sets are prepared, involving changes to the upper limbs (mirrored in the lower limbs), the left upper limb, and the right lower limb. A major challenge in localized modifications is maintaining kinematic consistency. Direct stitching (see supplementary materials) often introduces artifacts such as simultaneous hand and foot movements. To avoid inconsistent hip-limb coordination, we introduce upper-body influence on lower-body dynamics for automatic inter-joint conflict correction. By

replacing the rotations and positions of selected body parts with those from the target style, we achieve localized modifications. For each test sequence, a random target style is applied. RSMT [33] encodes style from full-body motion sequences via a convolutional neural network, for which we provide both original and modified inputs. In contrast, our method replaces the selected body part’s phase with that of the target style.

As shown in Table 2, our phase-aware replacement outperforms direct stitching in preserving limb coordination (see supplementary video). CVAE [32], without explicit style control, predicts the most probable motion. The similarity between RSMT (original) and RSMT (modified) suggests motion-sequence-based encoding has limited impact. PhaseMIB [28] struggles with body-part variations due to its teacher-forcing paradigm, which limits extrapolation beyond training data. In contrast, our part-wise phase representation and autoregressive generation enable dynamic

inter-limb coordination during synthesis.

4.3. Ablation Study on Style Encoder.

We evaluate the effectiveness of the body-part-phase-based style encoder in our framework, as shown in Table 3. In this study, we replace the style encoder with convolutional neural networks that utilize the full-body motion sequence. The construction of the test data is consistent with that described in Section 4.2. We also evaluate the effectiveness of the style encoder under conditions of body part style variation. When style encoding relies on motion sequences, it fails to effectively capture style information, leading to inferior motion quality compared to our framework. The results of the ablation experiments highlight the significance of style encoding based on body part phases, emphasizing its contribution to the effectiveness and quality of our framework.

4.4. Body Part Motion Adjustment

We scale the body part phases A and S by a factor and use the adjusted values to compute the phase per formula 1. The scaled phase serves as an input to the sampler, predicting the next frame’s phase and updating gating network parameters. To maintain coordination, unselected body parts may exhibit slight variations.

We evaluate three styles: *HighKnees*, *Swimming*, and *Flapping*. For each, representative motion segments are selected, with frames i and j marking the start and end. The first two rows of each column in the figures show motion snapshots at five sampled points, while the third row illustrates changes in key metrics from i to j (in Figure 5i, the ending frame extends 17 frames beyond j).

Amplitude Control. As shown in Figure 4, our framework adjusts motion amplitude by modifying phase amplitudes. For *HighKnees*, reducing lower limb phase amplitudes to 50% of their original values (Figure 4a) decreases knee height, compared to the unmodified version (Figure 4d). For *Swimming*, reducing upper limb phase amplitudes to 50% (Figure 4b) narrows the wrist distance, while Figure 4e shows the original. For *Flapping*, Figure 4f increases upper limb phase amplitudes to 250%, raising hand height compared to Figure 4c. Figures 4g–4i show the effect of different scaling factors on leg lift amplitude, hand distance, and hand height.

Frequency Control. Figure 5 illustrates the impact of modifying phase frequencies on motion speed. For the *HighKnees* style, increasing the lower limb phase frequency to 250% of its original value (Figure 5d) results in the knee reaching its peak height significantly faster compared to the unmodified motion (Figure 5a). This effect is quantitatively shown in Figure 5g, where the leg lift amplitude at different scaling factors is plotted over time. A

higher frequency accelerates movement, while slower frequencies cause the knee to reach a lower peak before descending to maintain consistency with the final keyframe. For the *Swimming* style, doubling the phase frequency of the upper limbs (Figure 5e) speeds up arm movement, making them reach target positions more quickly than in the unmodified version (Figure 5b). Figure 5h further illustrates how the distance between the hands varies under different frequency scaling factors, demonstrating that increased frequency leads to faster hand convergence. For the *Flapping* style, reducing the upper limb phase frequency to 50% of its original value (Figure 5c) slows down the arm motion, while Figure 5f shows the original unmodified pace. Despite these changes in motion speed, Figure 5i confirms that the amplitude remains consistent, as both the highest and lowest points of hand movement remain unaffected by frequency variations.

5. Conclusion

In this paper, we introduce a novel framework for stylized motion in-betweening with a focus on body-part-level control. Leveraging phase-related techniques and periodic autoencoders, our approach improves both the diversity and controllability of animated sequences. Experimental results demonstrate that our method outperforms existing approaches in generating realistic animations, enabling precise adjustments to individual limb movements while preserving overall motion coherence. These advancements establish our framework as a valuable tool for expressive motion synthesis, with applications in gaming, virtual reality, and beyond.

References

- [1] Dhruv Agrawal, Jakob Buhmann, Dominik Borer, Robert W Sumner, and Martin Guay. Skel-betweener: a neural motion rig for interactive motion authoring. *ACM Transactions on Graphics (TOG)*, 43(6):1–11, 2024. 2, 5
- [2] Okan Arikan and David A Forsyth. Interactive motion generation from examples. *ACM Transactions on Graphics (TOG)*, 21(3):483–490, 2002. 2
- [3] Philippe Beaudoin, Stelian Coros, Michiel Van de Panne, and Pierre Poulin. Motion-motif graphs. In *Proceedings of the 2008 ACM SIGGRAPH/Eurographics symposium on computer animation*, pages 117–126, 2008. 2
- [4] Jalil Chavez-Galaviz, Jianwen Li, Ajinkya Chaudhary, and Nina Mahmoudian. Asv station keeping under wind disturbances using neural network simulation error minimization model predictive control. *Journal of Field Robotics*, 41(6): 1797–1813, 2024. 5
- [5] Wenheng Chen, He Wang, Yi Yuan, Tianjia Shao, and Kun Zhou. Dynamic future net: Diversified human motion generation. In *Proceedings of the 28th ACM International Conference on Multimedia*, pages 2131–2139, 2020. 2

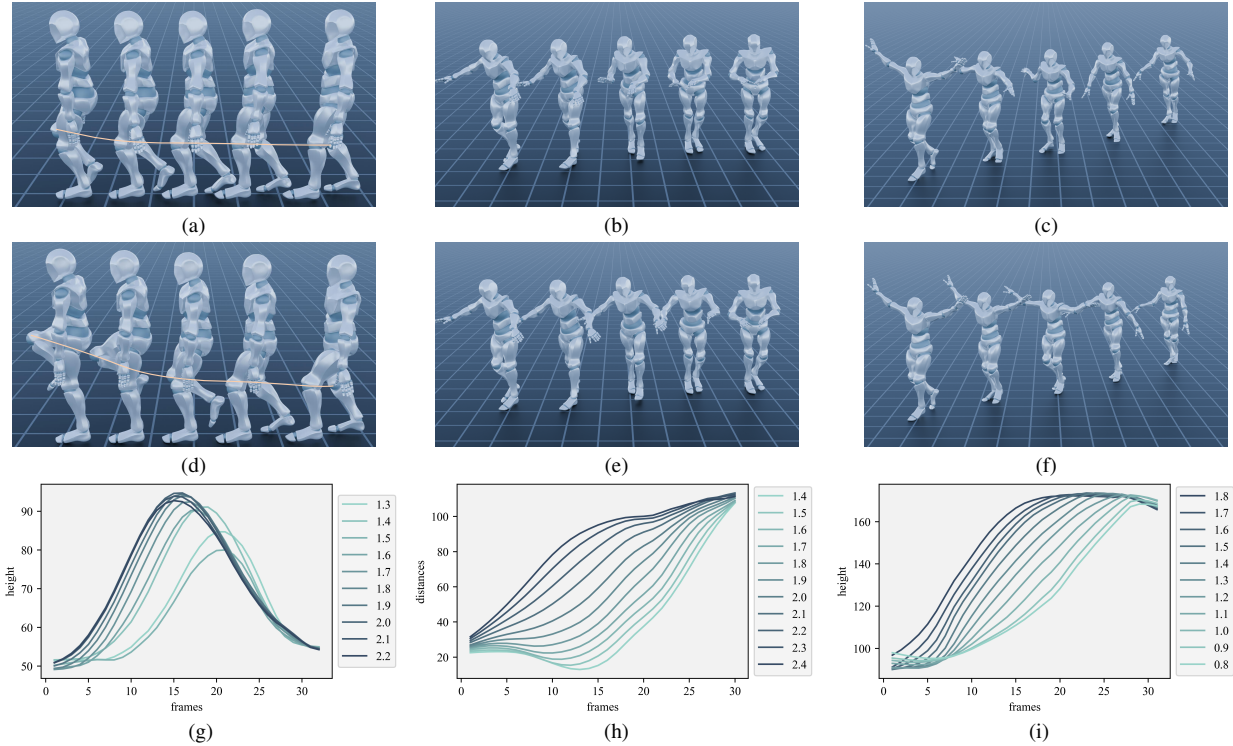


Figure 5. Results of adjusting the frequency of body part phases

- [6] Félix G Harvey and Christopher Pal. Recurrent transition networks for character locomotion. In *SIGGRAPH Asia 2018 Technical Briefs*, pages 1–4. 2018. [2](#)
- [7] Félix G Harvey, Mike Yurick, Derek Nowrouzezahrai, and Christopher Pal. Robust motion in-betweening. *ACM Transactions on Graphics (TOG)*, 39(4):60–1, 2020. [2](#), [3](#), [4](#), [5](#)
- [8] Chengan He, Jun Saito, James Zachary, Holly Rushmeier, and Yi Zhou. Nemf: Neural motion fields for kinematic animation. *Advances in Neural Information Processing Systems*, 35:4244–4256, 2022. [2](#)
- [9] Daniel Holden, Jun Saito, Taku Komura, and Thomas Joyce. Learning motion manifolds with convolutional autoencoders. In *SIGGRAPH Asia 2015 technical briefs*, pages 1–4. 2015. [2](#)
- [10] Daniel Holden, Jun Saito, and Taku Komura. A deep learning framework for character motion synthesis and editing. *ACM Transactions on Graphics (TOG)*, 35(4):1–11, 2016. [2](#), [5](#)
- [11] Daniel Holden, Taku Komura, and Jun Saito. Phase-functioned neural networks for character control. *ACM Transactions on Graphics (TOG)*, 36(4):1–13, 2017. [2](#), [3](#)
- [12] Deok-Kyeong Jang and Sung-Hee Lee. Constructing human motion manifold with sequential networks. In *Computer Graphics Forum*, pages 314–324. Wiley Online Library, 2020. [2](#)
- [13] Deok-Kyeong Jang, Soomin Park, and Sung-Hee Lee. Motion puzzle: Arbitrary motion style transfer by body part. *ACM Transactions on Graphics (TOG)*, 41(3):1–16, 2022. [5](#)
- [14] Mazeyu Ji, Xuanbin Peng, Fangchen Liu, Jialong Li, Ge Yang, Xuxin Cheng, and Xiaolong Wang. Exbody2: Advanced expressive humanoid whole-body control. *arXiv preprint arXiv:2412.13196*, 2024. [5](#)
- [15] Lucas Kovar, Michael Gleicher, and Frédéric Pighin. Motion graphs. In *Seminal Graphics Papers: Pushing the Boundaries, Volume 2*, pages 723–732. 2023. [2](#)
- [16] Sergey Levine, Jack M Wang, Alexis Haraux, Zoran Popović, and Vladlen Koltun. Continuous character control with low-dimensional embeddings. *ACM Transactions on Graphics (TOG)*, 31(4):1–10, 2012. [2](#)
- [17] Jiaman Li, Ruben Villegas, Duygu Ceylan, Jimei Yang, Zhengfei Kuang, Hao Li, and Yajie Zhao. Task-generic hierarchical human motion prior using vaes. In *2021 International Conference on 3D Vision (3DV)*, pages 771–781. IEEE, 2021. [2](#)
- [18] Peizhuo Li, Sebastian Starke, Yuting Ye, and Olga Sorkine-Hornung. Walkthedog: Cross-morphology motion alignment via phase manifolds. In *ACM SIGGRAPH 2024 Conference Papers*, pages 1–10, 2024. [5](#)
- [19] Hung Yu Ling, Fabio Zinno, George Cheng, and Michiel Van De Panne. Character controllers using motion vaes. *ACM Transactions on Graphics (TOG)*, 39(4):40–1, 2020. [2](#)
- [20] Chenhao Lu, Xuxin Cheng, Jialong Li, Shiqi Yang, Mazeyu Ji, Chengjing Yuan, Ge Yang, Sha Yi, and Xiaolong Wang. Mobile-television: Predictive motion priors for humanoid whole-body control. *arXiv preprint arXiv:2412.07773*, 2024. [5](#)
- [21] Ian Mason, Sebastian Starke, and Taku Komura. Real-time style modelling of human locomotion via feature-wise trans-

- formations and local motion phases. *Proceedings of the ACM on Computer Graphics and Interactive Techniques*, 5(1):1–18, 2022. 2, 3, 5
- [22] Jianyuan Min and Jinxiang Chai. Motion graphs++ a compact generative model for semantic motion analysis and synthesis. *ACM Transactions on Graphics (TOG)*, 31(6):1–12, 2012. 2
- [23] Clinton A Mo, Kun Hu, Chengjiang Long, and Zhiyong Wang. Continuous intermediate token learning with implicit motion manifold for keyframe based motion interpolation. In *Proceedings of the IEEE/CVF Conference on Computer Vision and Pattern Recognition*, pages 13894–13903, 2023. 2
- [24] Mathis Petrovich, Michael J Black, and Gül Varol. Action-conditioned 3d human motion synthesis with transformer vae. In *Proceedings of the IEEE/CVF International Conference on Computer Vision*, pages 10985–10995, 2021.
- [25] Davis Rempe, Tolga Birdal, Aaron Hertzmann, Jimei Yang, Srinath Sridhar, and Leonidas J Guibas. Humor: 3d human motion model for robust pose estimation. In *Proceedings of the IEEE/CVF international conference on computer vision*, pages 11488–11499, 2021. 2
- [26] Alla Safonova and Jessica K Hodgins. Construction and optimal search of interpolated motion graphs. In *ACM SIGGRAPH 2007 papers*, pages 106–es. 2007. 2
- [27] Yijun Shen, He Wang, Edmond SL Ho, Longzhi Yang, and Hubert PH Shum. Posture-based and action-based graphs for boxing skill visualization. *Computers & Graphics*, 69:104–115, 2017. 2
- [28] Paul Starke, Sebastian Starke, Taku Komura, and Frank Steinicke. Motion in-betweening with phase manifolds. *Proceedings of the ACM on Computer Graphics and Interactive Techniques*, 6(3):1–17, 2023. 3, 6, 7
- [29] Sebastian Starke, He Zhang, Taku Komura, and Jun Saito. Neural state machine for character-scene interactions. *ACM Transactions on Graphics*, 38(6):178, 2019. 3
- [30] Sebastian Starke, Yiwei Zhao, Taku Komura, and Kazi Zaman. Local motion phases for learning multi-contact character movements. *ACM Transactions on Graphics (TOG)*, 39(4):54–1, 2020. 3
- [31] Sebastian Starke, Ian Mason, and Taku Komura. Deepphase: Periodic autoencoders for learning motion phase manifolds. *ACM Transactions on Graphics (TOG)*, 41(4):1–13, 2022. 2, 3
- [32] Xiangjun Tang, He Wang, Bo Hu, Xu Gong, Ruifan Yi, Qilong Kou, and Xiaogang Jin. Real-time controllable motion transition for characters. *ACM Transactions on Graphics (TOG)*, 41(4):1–10, 2022. 2, 3, 4, 6, 7
- [33] Xiangjun Tang, Linjun Wu, He Wang, Bo Hu, Xu Gong, Yuchen Liao, Songnan Li, Qilong Kou, and Xiaogang Jin. Rsmt: Real-time stylized motion transition for characters. In *ACM SIGGRAPH 2023 Conference Proceedings*, pages 1–10, 2023. 2, 3, 5, 6, 7
- [34] He Wang, Kirill A Sidorov, Peter Sandilands, and Taku Komura. Harmonic parameterization by electrostatics. *ACM Transactions on Graphics (TOG)*, 32(5):1–12, 2013. 2
- [35] He Wang, Edmond SL Ho, and Taku Komura. An energy-driven motion planning method for two distant postures. *IEEE transactions on visualization and computer graphics*, 21(1):18–30, 2014. 2
- [36] He Wang, Edmond SL Ho, Hubert PH Shum, and Zhanxing Zhu. Spatio-temporal manifold learning for human motions via long-horizon modeling. *IEEE transactions on visualization and computer graphics*, 27(1):216–227, 2019. 2
- [37] Tianhao Wu, Jing Zhang, Min Gu, Jinling Jiang, Zhi Li, Chen Lin, and Yan Su. Analysis and verification of the temperature drift characteristics of mems resonant sensors during power-on startup. *IEEE Transactions on Instrumentation and Measurement*, 72:1–14, 2023. 5
- [38] Yuting Ye and C Karen Liu. Synthesis of responsive motion using a dynamic model. In *Computer Graphics Forum*, pages 555–562. Wiley Online Library, 2010. 2
- [39] He Zhang, Sebastian Starke, Taku Komura, and Jun Saito. Mode-adaptive neural networks for quadruped motion control. *ACM Transactions on Graphics (TOG)*, 37(4):1–11, 2018. 5
- [40] Haoyu Zhao, Hao Wang, Chen Yang, and Wei Shen. Chase: 3d-consistent human avatars with sparse inputs via gaussian splatting and contrastive learning. *arXiv preprint arXiv:2408.09663*, 2024. 2
- [41] Haoyu Zhao, Chen Yang, Hao Wang, Xingyue Zhao, and Wei Shen. Sg-gs: Photo-realistic animatable human avatars with semantically-guided gaussian splatting. *arXiv preprint arXiv:2408.09665*, 2024. 2
- [42] Yi Zhou, Jingwan Lu, Connelly Barnes, Jimei Yang, Sitao Xiang, et al. Generative tweening: Long-term inbetweening of 3d human motions. *arXiv preprint arXiv:2005.08891*, 2020. 3